

Randomized Maximum Likelihood via High-Dimensional Bayesian Optimization

Valentin Breaz¹ Richard Wilkinson¹

¹ School of Mathematical Sciences, University of Nottingham, Nottingham, United Kingdom

Abstract

Randomized Maximum Likelihood (RML) is an approximate posterior sampling methodology, widely used in Bayesian inverse problems with complex forward models, particularly in petroleum engineering applications. The procedure involves solving a multi-objective optimization problem, which can be challenging in high-dimensions and when there are constraints on computational costs. We propose a new methodology for tackling the RML optimization problem based on the high-dimensional Bayesian optimization literature. By sharing data between the different objective functions, we are able to implement RML at a greatly reduced computational cost. We demonstrate the benefits of our methodology in comparison with the solutions obtained by alternative optimization methods on a variety of synthetic and real-world problems, including medical and fluid dynamics applications. Furthermore, we show that the samples produced by our method cover well the high-posterior density regions in all of the experiments.

1. Introduction

We consider a Bayesian inverse problem, where the goal is to sample from the posterior distribution

$$p(x|\mathcal{D}) = \frac{p(\mathcal{D}|x)p(x)}{p(\mathcal{D})}$$

of the unknown parameters $x \in \mathbb{R}^D$ given the observed data $\mathcal{D} \in \mathbb{R}^m$. Typically, the likelihood is assumed to be a Gaussian distribution

$$\mathcal{D}|x \sim \mathcal{N}_m(f(x), \Sigma_{\text{obs}}),$$

where $f(x) : \mathbb{R}^D \rightarrow \mathbb{R}^m$ is known as the simulator, and is typically the deterministic solution to a partial differential equation (PDE) modelling an underlying physical process (Stuart, 2010). The covariance matrix Σ_{obs} is typically diagonal ($\Sigma_{\text{obs}} = \sigma^2 I_m$) and contains the modelling and observational errors. Bayesian inverse problems are employed in a variety of applications, such as climate modelling (Holden

et al., 2018), medical imaging (Dunlop & Stuart, 2015), material sciences (Iglesias et al., 2018), and petroleum engineering (Emerick & Reynolds, 2013). See Stuart (2010) for a comprehensive survey.

Randomized Maximum Likelihood (RML) was introduced by Oliver et al. (1996), as an approximate posterior sampling methodology. RML is formulated for the situation where the observations are subject to Gaussian distributed errors (i.e., a Gaussian likelihood) and where the prior distribution is also Gaussian: $x \sim \mathcal{N}_D(\mu, \Sigma)$. The algorithm proceeds by first perturbing the data and the prior mean, and then optimizing the unnormalised log-posterior using these perturbed values. See Algorithm 1.

Algorithm 1 Randomized Maximum Likelihood (RML)

n_{RML} : number of samples required

for $n \in [n_{RML}]$ **do**

1. Sample $\mathcal{D}_n \sim \mathcal{N}_m(\mathcal{D}, \Sigma_{\text{obs}})$ from the Gaussian likelihood
2. Sample $\mu_n \sim \mathcal{N}_D(\mu, \Sigma)$ from the Gaussian prior
3. Construct $\log p(\mathcal{D}|x)p(x)$ w.r.t. the randomizations (\mathcal{D}_n, μ_n)

$$O_n(x) := \log \mathcal{N}_m(f(x)|\mathcal{D}_n, \Sigma_{\text{obs}}) + \log \mathcal{N}_D(x|\mu_n, \Sigma) \quad (1)$$

4. Obtain x_n^* as the maximizer $x_n^* = \arg \max_x O_n(x)$.

end for

Here, we use the notation $[n_{RML}] = \{1, 2, \dots, n_{RML}\}$. Thus RML solves n_{RML} optimization problems, each with a different objective function, $O_n(x)$. The resulting solutions $\{x_n^*\}_{n=1}^{n_{RML}}$ are regarded as approximate samples from the posterior distribution $p(x|\mathcal{D})$; the samples are only exact draws from the posterior when the simulator $f(x)$ is linear (see Appendix A for a proof in the linear case). Some of the practical success in a variety of petroleum engineering applications (Gao & Reynolds, 2006; Emerick & Reynolds, 2013) can be associated with the “weakly nonlinear” nature of the simulators used (Skjervheim & Evensen, 2011; Evensen, 2018). Additional care needs to be taken in more challenging scenarios, such as multi-modal posteriors with highly nonlinear simulators, and there is a series of works which addresses these challenges both theoretically and empirically (Bardsley et al., 2014; Oliver, 2015; Ba et al.,

2021). Nonetheless, good practical performance has been observed for nonlinear (deep) neural network parametrized simulators in a series of more recent petroleum engineering publications (Liu et al., 2019; Tang et al., 2020).

Instead of focusing on the accuracy of the approximate samples $\{x_n^*\}_{n=1}^{n_{RM}}L$ with respect to the true posterior, we address solving the optimization problems (1) efficiently in the challenging case of a high-dimensional input space \mathbb{R}^D . We focus on the specific scenario where the log-likelihood

$$\log p(\mathcal{D}|x) \propto L(x) := -\|\mathcal{D} - f(x)\|_{\Sigma_{\text{obs}}}^2 \quad (2)$$

has a low-dimensional active subspace (Constantine et al., 2015), where we use the notational convention that $\|y\|_{\Sigma}^2 = y^T \Sigma y$. In other words, when $L(x) \approx g(A^T x)$, where $g : \mathbb{R}^d \rightarrow \mathbb{R}$ with $d \ll D$, and $A \in \mathbb{R}^{D \times d}$ is a semi-orthogonal matrix (i.e., $A^T A = I_d$). See Constantine et al., 2013, Constantine et al., 2015, Seshadri et al., 2018, and Wycoff et al., 2019 for theoretical considerations and practical applications of active subspaces. As pointed out in Constantine et al. (2015), many log-likelihoods used in Bayesian inverse problems possess such a low-dimensional structure.

The following is a list of assumptions and challenges that are commonly faced in applied problems, and which motivate the methodological developments in this paper:

1. Computational constraints mean that we are limited to at most N simulator evaluations. For complex simulators, N may be small.
2. We do not have access to gradients of the simulator. Automatic differentiation methods can fail for codes which involve long iterations, such as differential equation solvers. Although progress is being made (see e.g., Yashchuk, 2020; Ma et al., 2021) many organizations rely on legacy code and may lack the resource to rewrite complex simulators.
3. Although we assume an active subspace A exists, we do not have access to A , and moreover, we do not have sufficient budget to estimate it from $\{x_i, L(x_i)\}_{i=1}^N$.
4. Even though the log-likelihood has a low-dimensional active subspace, the prior might not have such a structure, for example when $x \sim \mathcal{N}(0, I_D)$.

If we ignore the prior and the multi-objective nature of our problem for now, the task of maximizing an objective $O(x) \approx g(A^T x)$ (in this case, the log-likelihood) under the assumptions mentioned above is common in the high-dimensional Bayesian Optimization (HD-BO) literature, which is key to our work.

Bayesian Optimization (BO, i.e. finding $\arg \max_x O(x)$ using a Gaussian process approximation $g_{\text{GP}}(x) \approx O(x)$) is based on a standard exploration-exploitation principle.

Namely, an acquisition function based on $g_{\text{GP}}(x)$ is used such that in the exploration phase, the target function $O(x)$ is explored globally, whereas in the exploitation phase points \tilde{x} which are likely to satisfy $\tilde{x} = \arg \max_x O(x)$ are sampled, until the maximum is eventually found. See Frazier (2018) for a comprehensive introduction to BO, and Rasmussen & Williams (2005) for an introduction to Gaussian processes (GPs).

GPs are known to deal well with small training budgets, but may struggle with high input dimensionality D (Liu & Guillas, 2016), as the covariance function typically relies upon the distance between inputs. As a result, the HD-BO literature mostly deals with the prevalent case where the approximation $g_{\text{GP}}(x) \approx O(x)$ is unsatisfactory. In our setting where an active subspace exists but is unknown, the most common solution is the use of random embeddings, R , instead of the true low-dimensional embedding A ; see Wang et al. (2013) for the seminal work on this topic. Here we abuse notation, and use R to denote both the random subspace and the $D \times d_e$ projection matrix from \mathbb{R}^D into that space.

Algorithm 2 presents a generic HD-BO algorithm with random embeddings. The random embedding, R , transforms the original high-dimensional BO problem $O(x) \sim \text{GP}$ for $x \in \mathbb{R}^D$ into a low-dimensional BO problem $O(Ry) \sim \text{GP}$ for $y \in \mathbb{R}^{d_e}$. In other words, instead of trying to maximize $O(x)$, we try to maximize $O(Ry)$, which is the objective function on the subspace R .

Algorithm 2 Generic HD-BO with random embeddings

M : number of evaluations of $O(\cdot)$ possible given the computational budget;
 d_e : chosen dimensionality of the embedding R ;
 $R \in \mathbb{R}^{D \times d_e}$: random embedding;
 m_0 : initial training points $\{y_i, O(Ry_i)\}_{i=1}^{m_0}$, with $y_i \in \mathbb{R}^{d_e}$
for $m \in \{m_0 + 1, \dots, M\}$ **do**
 1. Construct a GP approximation $O(Ry) \sim \text{GP}$ using the available objective function evaluations $\{y_i, O(Ry_i)\}_{i=1}^{m-1}$
 2. Select $y_m = \arg \max_y a_m(y)$ as the maximizer of a BO acquisition function for $O(Ry) \sim \text{GP}$
 3. Update the training data to $\{y_i, O(Ry_i)\}_{i=1}^m$.
end for
Obtain $x_* = Ry_{m_*}$ as the maximizer

$$m_* = \arg \max_m O(Ry_m), \quad m \leq M.$$

In practice, we can use multiple random projections (Wang et al., 2013) giving maximizers x_*^1, \dots, x_*^K , and select the quantity $x_* := \arg \max_{x_*^k} O(x_*^k)$ that gives the largest objective function value.

1.1. Contributions

In this paper we

- propose a new methodology for maximizing the RML objective functions (1) via HD-BO (algorithms 3 and 4);
- propose a natural way to exploit the shared simulator $f(x)$ which is present in all of the objective functions (1), as well as an adjustment needed to incorporate a prior distribution without a low-dimensional structure;
- show that in the limited budget setting, our methodology often outperforms alternative gradient-free optimization methods, demonstrating this in a series of synthetic and real-world experiments;
- visualize the posterior distribution in the active subspace (Constantine et al., 2015), together with the samples produced by our methodology; we show that the samples are indeed close to ‘true’ RML samples (collected via an infinite computational budget), while also covering well the high posterior density regions.

1.2. Related work

Although there is an extensive literature for HD-BO with random embeddings, which offers theoretical guarantees and good practical performance (see, e.g., Wang et al., 2013; Nayebi et al., 2019 and Letham et al., 2020, which includes a recent survey on the topic), there is no methodology designed for posterior sampling. Yet RML is a natural way to use HD-BO for high-dimensional posterior sampling.

The closest related work is Hamdi et al. (2017), where BO is compared with alternative gradient-free optimization methods for maximizing the log-likelihood in a variety of low-dimensional experiments related to petroleum engineering. We extend their work by considering the multi-objective setting (n_{RML} randomized log-likelihoods) in order to do posterior sampling, as well as considering the challenging high-dimensional case and incorporating high-dimensional priors.

The use of GPs for posterior sampling in low-dimensional experiments can be found in the active learning methodology literature, where the aim is to generate training points from high-posterior density regions (Kandasamy et al., 2017; Wang & Li, 2017; Takhtaganov & Müller, 2018). Regarding high-dimensional experiments, GPs have been used in cases where the prior distribution had a low-dimensional structure which was amenable to dimension reduction (Bilionis & Zabaras, 2014; Tian et al., 2017), or when the simulation budget was large enough to estimate the active subspace from data $\{x_i, L(x_i)\}_{i=1}^N$ (Bilionis et al., 2016). Alternatively, (deep) neural networks have been used for Bayesian

inversion experiments in various settings (Ardizzone et al., 2018; Goh et al., 2019; Siahkoochi et al., 2021). In relation to our work, Tang et al. (2020) uses a deep neural network surrogate model for the simulator, together with a standard optimization routine for maximizing the RML objectives using a large number of surrogate evaluations, in a challenging high-dimensional petroleum engineering experiment.

One widely employed methodology for inversion under computational budget constraints is an iterative Kalman filter type update, which moves particles from the prior distribution towards samples from the posterior distribution of the inverse problem. One of the most popular versions is the Ensemble Kalman Inversion (EKI) algorithm; see Iglesias & Yang (2020) for a recent survey and state-of-the-art results, and Ju et al. (2018), which extends the method by using a GP approximation for the simulator within EKI that is updated after every Kalman iteration. While EKI is mostly used to target the solution in the classical inverse problem sense (i.e., x_{true} which generated the observations via $\mathcal{D} = f(x_{true}) + \epsilon$), an alternative line of work targets the full posterior distribution $p(x|\mathcal{D})$ in a methodology known as Ensemble Kalman Sampler (EKS) Garbuno-Inigo et al. (2020), together with its other variants (Garbuno-Inigo et al., 2019; Reich & Weissmann, 2019). GP models have been used together with the EKS methodology in various settings (Cleary et al., 2021; Duncan et al., 2021), showing improved results compared with vanilla EKS.

Another methodology related to RML for stochastic simulators is reverse sampling (Forneron & Ng, 2015) and Optimization Monte Carlo (OMC) (Meeds & Welling, 2015). In particular, in Algorithm 3 in the Robust OMC algorithm of Ikononov & Gutmann (2019), a GP model is used for a collection of randomized objectives $R_j(x)$ maximized with BO. The GP approximations are used as a sampling tool at every iteration. It would be interesting to see if these ideas can be applied in the deterministic simulator setting considered here.

2. Methodology

Firstly, we consider the simpler setting of a uniform prior, $x \sim U[a_i, b_i]_{i=1}^D$, where $[a_i, b_i]_{i=1}^D := [a_1, b_1] \times \dots \times [a_D, b_D]$. In this case, the posterior distribution is proportional to the likelihood, and using our active subspace assumption the RML objective functions (1) become

$$O_n(x) := \log \mathcal{N}_m(f(x)|\mathcal{D}_n, \Sigma_{\text{obs}}) \approx g_n(A_n^T x), \quad (3)$$

where the objective functions now need to be maximized over the prior support $[a_i, b_i]_{i=1}^D$.

A naive strategy would be to perform HD-BO independently for each objective function (3), i.e., train GP approximations

$$g_{\text{GP}}^{(n)}(y) \approx O_n(Ry), \text{ for } n \in [n_{RML}]. \quad (4)$$

Assuming that each HD-BO procedure is run over T iterations, this strategy will result in a collection of Tn_{RML} simulations $\{(y_t^n, f(Ry_t^n))\}$ for $t \in [T]$ and $n \in [n_{RML}]$. Note that the limited budget, N , constrains us to $T \leq N/n_{RML}$ iterations for each objective.

However, note that every data point $\{(y_t^n, f(Ry_t^n))\}$ can be shared by all the objectives (3). Since all the objective functions $O_n(x)$ have similar structure and are based on the same underlying simulator $f(x)$, we expect that the exploration stage can be performed at once for all objective functions, which can potentially lead to a great speed-up in HD-BO convergence. For example, we could run HD-BO for $O_1(x)$ (T_1 iterations say), and then reuse the training data $\{(y_t^1, f(Ry_t^1))\}$ to warm-start/speed-up convergence for $O_2(x)$ ($T_2 \ll T_1$). Whilst this is an attractive strategy, it poses the difficulty of having to choose a stopping time T_n for every objective.

To circumvent the challenges mentioned above, we propose our procedure in Algorithm 3, and a schematic representation of the first two iterations of this is shown in Figure 1.

Algorithm 3 HD-BO-RML with uniform priors

N : max possible number of evaluations of $f(\cdot)$;
 d_e : choice of embedding dimensionality;
 $R_1, \dots, R_K \in \mathbb{R}^{D \times d_e}$: collection of random embeddings;
 $n_0 \times K$ initial points: $\{y_i^k, f(R_k y_i^k)\}_{i=1}^{n_0}$, with $y_i^k \in \mathbb{R}^{d_e}$, $k \in [K]$;
for $k \in \{1, \dots, K\}$ **do**
 for $n \in \{n_0 + 1, \dots, \lfloor N/K \rfloor\}$ **do**
 1. Set $n' := n \bmod n_{RML}$
 2. Construct a GP approximation to $O_{n'}(R_k y)$ using simulations $\{y_i^k, f(R_k y_i^k)\}_{i=1}^{n-1}$
 3. Select $y_n^k = \arg \max_y a_n^k(y)$ as the maximizer of a BO acquisition function using the GP approximation
 4. Perform simulation $f(R_k y_n^k)$ and update the shared simulation ensemble to $\{y_i^k, f(R_k y_i^k)\}_{i=1}^n$.
 end for
end for
for $n \in \{1, \dots, n_{RML}\}$ **do**
 1. Obtain $x_n^* = R_{k_*} y_{m_*}^{k_*}$ as the maximizer

 $k_*, m_* = \arg \max_{k,m} O_n(R_k y_m^k)$, $k \in [K], m \leq \lfloor N/K \rfloor$
end for

As suggested by Wang et al. (2013), we use a collection of K interleaved random embeddings instead of a single random embedding for the entire procedure. The algorithm is based on a cyclic pass through all the objective func-

tions (3), where for every random embedding $k \in [K]$, the simulations $\{(y_m^k, f(R_k y_m^k))\}_{m=1}^n$ collected up to some iteration n will serve as basis for the training set used in the next iteration, where the objective function $O_{(n+1)'}(x)$ is considered, with $(n+1)' := n+1 \bmod n_{RML}$.

As discussed above, we expect that the exploration stage will be performed simultaneously for all objective functions, as opposed to n_{RML} times in the naive strategy (4). When reaching the exploitation phase for $O_{n'}(x)$, it is likely that $O_{(n+1)'}(x)$ will also benefit from the shared basis for the training data $\{(y_m^k, f(R_k y_m^k))\}_{m=1}^n$ with $O_{n'}(x)$ and enter the exploitation phase. Also, due to the cyclic pass through all the objectives, we sidestep the difficulty of having to choose a stopping time T_n for every objective. Finally, we select the HD-BO-RML samples x_n^* for $n \in [n_{RML}]$ to be the maximizers of the n_{RML} objective functions (3) out of all the points selected by our procedure.

We now address the case of a Gaussian prior distribution, $x \sim \mathcal{N}_D(\mu, \Sigma)$. Using again the active subspace assumption, the objective functions (1) become:

$$O_n(x) = L_n(x) + \log p_n(x) \approx g_n(A_n^T x) + \log \mathcal{N}_D(x | \mu_n, \Sigma),$$

where $L_n(x) := \log \mathcal{N}_m(f(x) | \mathcal{D}_n, \Sigma_{\text{obs}})$. Due to the potential lack of low-dimensional structure in the prior, as for example if $x \sim \mathcal{N}(0, I_D)$, running HD-BO by modelling $O_n(Ry)$ as a GP might be unsatisfactory, and hence we cannot simply use the algorithm from the uniform prior case. Nonetheless, if we try to ignore the prior and use Algorithm 3 for the log-likelihood alone, we can still incorporate the prior in the final step:

$$k_*, m_* = \arg \max_{k,m} O_n(R_k y_m^k), \quad k \in [K], m \leq \lfloor N/K \rfloor.$$

This can lead to two obvious problems: we select either points of high-likelihood but low-prior (from the exploitation stage), or points of low-likelihood but reasonably high-prior (from the exploration stage). In our practical experiments, we encountered the second problem.

Our proposed procedure is given in Algorithm 4, as an ad-hoc fix to the issue mentioned above. While we keep performing HD-BO with respect to the log-likelihood as in Algorithm 3, we try to increase the prior value for the selected points of potentially high-likelihood $x_0 = R_k y_n^k$ by performing local optimization in the high-dimensional space \mathbb{R}^D , starting from x_0 . Note that the local maximization of $p_{n'}(x)$ does not require simulator evaluations and can be performed efficiently by using fast gradient-based optimization methods.

$$\begin{array}{c}
\begin{array}{cccc}
& 1 & \dots & n & n+1 \\
O_1(y) & \left(\begin{array}{c} y_1, O_1(y_1) \\ \vdots \\ y_n, O_1(y_n) \end{array} \right. & \left. \begin{array}{c} \vdots \\ y_n, O_1(y_n) \\ y_{n+1}, O_1(y_{n+1}) \end{array} \right) \\
O_2(y) & \left(\begin{array}{c} y_1, O_2(y_1) \\ \vdots \\ y_n, O_2(y_n) \end{array} \right. & \left. \begin{array}{c} \vdots \\ y_n, O_2(y_n) \\ y_{n+1}, O_2(y_{n+1}) \end{array} \right) \\
\vdots & \left(\begin{array}{c} \vdots \\ \vdots \\ \vdots \end{array} \right. & \left. \begin{array}{c} \vdots \\ \vdots \\ \vdots \end{array} \right) \\
O_M(y) & \left(\begin{array}{c} y_1, O_M(y_1) \\ \vdots \\ y_n, O_M(y_n) \end{array} \right. & \left. \begin{array}{c} \vdots \\ y_n, O_M(y_n) \\ y_{n+1}, O_M(y_{n+1}) \end{array} \right)
\end{array} \rightarrow \begin{array}{cccc}
& 1 & \dots & n & n+1 \\
\left(\begin{array}{c} y_1, O_1(y_1) \\ y_1, O_2(y_1) \\ \vdots \\ y_1, O_M(y_1) \end{array} \right. & \left. \begin{array}{c} \vdots \\ \vdots \\ \vdots \\ \vdots \end{array} \right) & \left(\begin{array}{c} y_{n+1}, O_1(y_{n+1}) \\ y_{n+1}, O_2(y_{n+1}) \\ \vdots \\ y_{n+1}, O_M(y_{n+1}) \end{array} \right) & \left(\begin{array}{c} y_{n+2}, O_1(y_{n+2}) \\ y_{n+2}, O_2(y_{n+2}) \\ \vdots \\ y_{n+2}, O_M(y_{n+2}) \end{array} \right)
\end{array}
\end{array}$$

Figure 1. To condense notation, we write $n := n_0$ for the initial points and $M := n_{RML}$ for the RML objectives. Also, we suppress the superscript k corresponding to the random embedding R_k , i.e., $y_p := y_p^k$ and $O_m(y) := O_m(R_k y)$ for $p \in [n]$ and $m \in [M]$. From top to bottom, according to the arrows: first HD-BO iteration to collect $y_{n+1} := y_{n+1}^k = \arg \max_y a_{n+1}^k(y)$ from $O_1(y) \sim \text{GP}$, then perform $f(R_k y_{n+1}^k)$ which generates data points $y_{n+1}, O_m(y_{n+1}) := y_{n+1}^k, O_m(R_k y_{n+1}^k)$ for all $m \in [M]$; second HD-BO iteration to collect $y_{n+2} := y_{n+2}^k = \arg \max_y a_{n+2}^k(y)$ from $O_2(y) \sim \text{GP}$, then perform $f(R_k y_{n+2}^k)$ which generates data points $y_{n+2}, O_m(y_{n+2}) := y_{n+2}^k, O_m(R_k y_{n+2}^k)$ for all $m \in [M]$.

Algorithm 4 HD-BO-RML with Gaussian priors

N : max possible number of evaluations of $f(\cdot)$;
 d_e : choice of embedding dimensionality;
 $R_1, \dots, R_K \in \mathbb{R}^{D \times d_e}$: collection of random embeddings;
 $n_0 \times K$ initial points: $\{y_i^k, f(R_k y_i^k)\}_{i=1}^{n_0}$, with $y_i^k \in \mathbb{R}^{d_e}$, $k \in [K]$;
for $k \in \{1, \dots, K\}$ **do**
 for $n \in \{n_0 + 1, \dots, \lfloor N/2K \rfloor\}$ **do**
 1. Let $n' := n \bmod n_{RML}$
 2. Construct a GP approximation to $L_{n'}(R_k y)$ using simulations $\{y_i^k, f(R_k y_i^k)\}_{i=1}^{n-1}$
 3. Select $y_n^k = \arg \max_y a_n^k(y)$ as the maximizer of a BO acquisition function using the GP approximation
 4. Perform $f(R_k y_n^k)$ and update the shared simulation ensemble to $\{y_i^k, f(R_k y_i^k)\}_{i=1}^n$
 5. Perform local optimization with respect to the prior and select $z_n^k = \arg \max_{x \in B} p_{n'}(x)$, where $B \in \mathbb{R}^D$ is a box centered at $x_0 = R_k y_n^k$.
 end for
end for
for $n \in \{1, \dots, n_{RML}\}$ **do**
 1. Obtain $x_n^* = z_{m_*}^{k_*}$ as the maximizer

 $k_*, m_* = \arg \max_{k, m} O_n(z_m^k)$, $k \in [K], m \leq \lfloor N/2K \rfloor$
end for

The resulting solution $z_n^k = \arg \max_{x \in B} p_{n'}(x)$ tries to achieve a trade-off between high-likelihood and high-prior; in this regard, the size of the local optimization box B is crucial and an important avenue for future work. For the experiments presented here, we have restricted the number of steps performed by the global optimization routine CMA-ES (Hansen et al., 2019), which started at the initial point $x_0 = R_k y_n^k$. See Appendix B.1 for more implementation details.

3. Experiments

3.1. Setup

We have performed a collection of experiments to show that our proposed algorithms can be successfully employed in a variety of synthetic and real-world Bayesian inverse problems. All the experiments use simulators which can be found on the Active Subspaces github page maintained by Constantine & Howard. Unless otherwise stated, we consider a uniform prior distribution $p(x)$ for all parameters; the measurements

$$\mathcal{D} = f(x_{true}) + \epsilon$$

have a noise level of 5% ($\sigma = 5\% \cdot f(x_{true})$) and x_{true} is sampled from $p(x)$. Note that for some of the experiments, a random sample $x_{true} \sim p(x)$ can lead to non-informative measurements \mathcal{D} , i.e. the posterior $p(x|\mathcal{D})$ is

very similar to the uniform prior $p(x)$, and in this case the optimization landscape for RML is uninteresting. To avoid this, we selected x_{true} samples which led to a significant difference between the prior and posterior. For each experiment, the resulting log-likelihood has been shown to have a two-dimensional active subspace, $L(x) \approx g(A^T x)$ with $g : \mathbb{R}^2 \rightarrow \mathbb{R}$. We present results for four simulators:

- Elliptic-PDE simulator $f : \mathbb{R}^{100} \rightarrow \mathbb{R}^7$ with measurements noise level of 1% and standard Gaussian prior $x \sim \mathcal{N}_{100}(0, I)$ (Constantine et al., 2015). This setup is common in many Bayesian inverse problems, including when non-Gaussian features $T(x)$ (e.g. channelized permeability fields in geology) generate the observations $\mathcal{D} = f(T(x)) + \epsilon$ (Iglesias et al., 2015).
- Ebola: $f : \mathbb{R}^8 \rightarrow \mathbb{R}$, an 8-parameter dynamical system model for the geographic spread of Ebola in Liberia (Diaz et al., 2016).
- MHD: $f : \mathbb{R}^5 \rightarrow \mathbb{R}$, a 5-parameter magnetohydrodynamics power generation model (Glaws et al., 2016).
- HIV long-term model: $f : \mathbb{R}^{27} \rightarrow \mathbb{R}$ is the cell count at time $t = 24$ (Loudon & Pankavich, 2016); the log likelihood has a one-dimensional active subspace, $L(x) \approx g(A^T x)$ with $g : \mathbb{R} \rightarrow \mathbb{R}$.

All the experiments use the Gaussian Process Upper Confidence Bound (GP-UCB) acquisition function (Srinivas et al., 2009), that is

$$a_n^k(y) = \mu_n^k(y) + \beta \sigma_n^k(y),$$

where $\mu_n^k(y)$ is the GP predictive mean which tries to approximate the log-likelihood $L_{n'}(R_k y)$, and $\sigma_n^k(y)$ represents the GP predictive uncertainty. This acquisition function has been studied in the HD-BO literature with random embeddings (Wang et al., 2013), and it was the first acquisition function for which theoretical guarantees were proven in the BO literature (Srinivas et al., 2009). We choose $\beta = 3$ for all experiments as a heuristic to facilitate a more exploratory behaviour, as the objective functions change iteratively from $O_{n'}(y)$ to $O_{(n+1)'}(y)$, but more principled approaches for choosing β from BO literature could also be used. The GP models use a standard squared-exponential covariance function (RBF kernel), i.e. $\text{Cov}(O(Ry_1), O(Ry_2)) := o^2 \exp\left(-\frac{\|y_1 - y_2\|^2}{2l^2}\right)$ for some objective function $O(Ry)$ and trainable hyperparameters o and l , known as the outputscale and lengthscale, respectively. They are trained at every iteration with a standard LBFGS algorithm, performed for 5 steps with learning rate 0.1.

For the random embeddings R_k , each row is sampled independently from the uniform distribution on the unit hypersphere \mathbb{S}^{d_e-1} , as suggested in (Binois, 2015; Letham

et al., 2020) (if $r \sim \mathcal{N}(0, I_{d_e})$, then $r/\|r\|$ is uniformly distributed on \mathbb{S}^{d_e-1}). In the case of a uniform prior $x \sim U[a_i, b_i]_{i=1}^D$, we constrain the maximization of the acquisition function to make sure that $R_k y$ projects back to the correct prior box via the transformation $[a_i, b_i]_{i=1}^D \rightarrow [-1, 1]^D$, followed by

$$\max_{y \in \mathbb{R}^{d_e}} a_n^k(y) \quad \text{subject to } -1 \leq (R_k y)_d \leq 1 \text{ for all } d \in [D],$$

as suggested in Letham et al. (2020). This constrained optimization is performed by SciPy’s COBYLA routine.

We have used the unconstrained CMA-ES optimization algorithm to maximize the acquisition function in the case of a Gaussian prior. More concretely, we start at $\mathbf{0}_{d_e}$ and set up a standard deviation of $\sqrt{d_e}$ for the CMA-ES optimization search, motivated by the heuristic that $y \in [-\sqrt{d_e}, \sqrt{d_e}]^{d_e}$ is likely to project back to $R_k y \in [-1, 1]^D$, and our prior $x \sim \mathcal{N}(0, I_D)$ has standard deviation 1. This heuristic was introduced by Wang et al. (2013) for random embeddings R with independent $\mathcal{N}(0, 1)$ entries, but our unit hypersphere random embeddings R_k can be obtained by normalizing the rows of R , as described in the previous paragraph.

We compare our algorithms to the following alternative gradient-free optimization methods:

- BOBYQA (Powell, 2007) - this algorithm was used for method comparison versus HD-BO in the experiments from Eriksson et al. (2019).
- CMA-ES (Hansen et al., 2019) - this algorithm was for method comparison versus HD-BO in the experiments from Eriksson et al. (2019) and Letham et al. (2020).
- Random design - standard baseline algorithm, present for method comparison in all the BO and HD-BO works.

We are interested in the method that finds points with the highest mean return, i.e., largest

$$\frac{1}{n_{RML}} \sum_{n=1}^{n_{RML}} O_n(x_n^*), \quad (5)$$

where x_n^* is the approximate maximizer of $O_n(x)$ as selected by the different methods considered.

3.2. Results

Table 1 gives the mean return (5) and its standard deviation over 5 optimization trials, and Figure 2 shows the (negative) mean returns for various budgets, averaged over the same 5 trials. Note that each experiment has a fixed set of measurements \mathcal{D} and thus a fixed set of RML objectives (1); the variance over the 5 trials comes from different optimization

Table 1. Mean return (5), together with the standard deviation over 5 trials. In bold, we outline the best competing method, together with the methods that outperform the best method in at least one trial. The oracle results are obtained with an infinite computational budget (i.e., infinite number of simulations) and are not part of the competing methods. We write PDE for the Elliptic-PDE simulator.

	PDE	EBOLA	MHD	HIV
RANDOM	-173.9 ± 1.0	$-1.0 \cdot 10^{-3} \pm 5.5 \cdot 10^{-4}$	$-4.0 \cdot 10^{-3} \pm 3.8 \cdot 10^{-3}$	$-1.6 \cdot 10^{-5} \pm 3.9 \cdot 10^{-6}$
BOBYQA	-169.3 ± 8.2	$-3.1 \cdot 10^{-6} \pm 2.8 \cdot 10^{-6}$	$-2.6 \cdot 10^{-7} \pm 2.7 \cdot 10^{-7}$	$-4.5 \cdot 10^{-2} \pm 7.3 \cdot 10^{-2}$
CMA-ES	-167.8 ± 5.0	$-9.7 \cdot 10^{-5} \pm 5.2 \cdot 10^{-5}$	$-3.3 \cdot 10^{-4} \pm 3.1 \cdot 10^{-4}$	$-6.7 \cdot 10^{-6} \pm 2.8 \cdot 10^{-6}$
HD-BO-RML	-132.2 ± 0.9	$-6.3 \cdot 10^{-5} \pm 6.8 \cdot 10^{-5}$	$-1.4 \cdot 10^{-5} \pm 1.9 \cdot 10^{-5}$	$-1.4 \cdot 10^{-5} \pm 1.3 \cdot 10^{-5}$
MAXIMUM (ORACLE)	-99.73	$-3.3 \cdot 10^{-15}$	0.0	$-4.6 \cdot 10^{-14}$

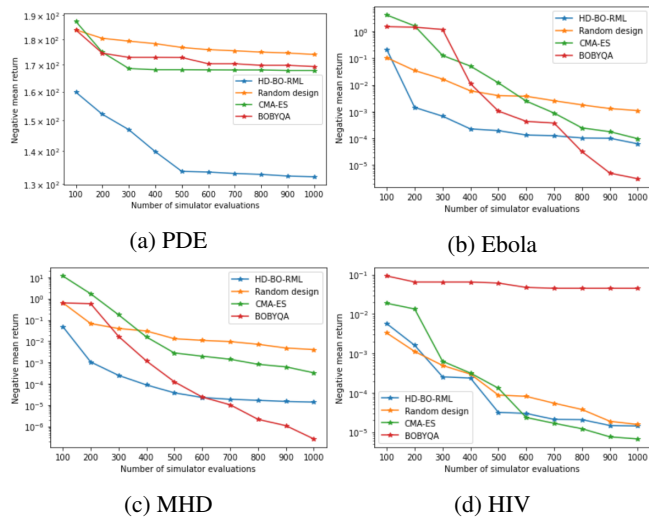


Figure 2. Averaged over the 5 trials presented in Table 1, we plot negative mean returns (5) (lower values are better). We do not plot the standard errors over the 5 trials, as they are not particularly insightful and can cause errors for the log-scale plots.

runs (e.g. different starting points for BOBYQA, different random embeddings used for HD-BO-RML).

Each trial has a budget of $N = 1000$ simulations in order to find $n_{RML} = 20$ samples. As n_{RML} grows, HD-BO-RML has an increasing advantage over the other methods, and so we have chosen a deliberately small number of samples, towards the lower end of what might be considered a useful number of posterior samples, in order to demonstrate that even in simple problems there is an advantage in using our approach. We use the libraries Py-BOBYQA (Cartis et al., 2018) and pycma (Hansen et al., 2019) for BOBYQA and CMA-ES, respectively, with default settings; see Appendix B.2 for more details on the implementation. Since BOBYQA and CMA-ES cannot share data between different objectives $O_i(x)$ and $O_j(x)$, unlike HD-BO-RML which shares data through the common simulator via the GP training sets, we employ BOBYQA and CMA-ES independently for each objective $O_n(x)$ for $n \in [n_{RML}]$, using

50 simulator evaluations per objective to stay within budget. Similar to HD-BO-RML, we select the RML samples for BOBYQA and CMA-ES, respectively, to be the points of largest mean return (5) out of all the $N = 1000$ simulator evaluations, instead of picking the samples from the final iterations of $O_n(x)$ for $n \in [n_{RML}]$ from the 50 simulator evaluations. For HD-BO-RML, we use $K = 10$ random embeddings with $d_e = d + 1$ ($d_e = d$ for Elliptic-PDE) and $n_0 = 5$ initial points (see Appendix B.3 for more details on these choices). Finally, the random design samples N points from $p(x)$, and returns the points of largest mean return (5).

Elliptic-PDE simulator. For this challenging high-dimensional experiment with a Gaussian prior, HD-BO-RML is the only best performing method at full budget (Table 1), as well as for a smaller number of simulator evaluations (Figure 2).

Ebola. BOBYQA and HD-BO-RML are the best methods at full budget, up to one standard deviation (Table 1). On average, HD-BO-RML works best in the smaller data regime $N \leq 500$, while BOBYQA works best for $N \geq 900$ (Figure 2).

MHD. BOBYQA is the best method at full budget up to one standard deviation, although it is outperformed by HD-BO-RML in one trial (Table 1). On average, HD-BO-RML works best in the smaller data regime $N \leq 400$, while BOBYQA works best for $N \geq 800$ (Figure 2).

HIV. CMA-ES is the best method at full budget up to one standard deviation, although it is outperformed by HD-BO-RML in three trials and by the random design in one trial (Table 1). BOBYQA fails due to small budget with respect to the input dimensionality.

Note that there is a significant performance gap between the competing methods (which all have budget constraints) and the oracle results obtained by numerical optimization without constraints on the number of simulations available; we refer to the oracle results as the ‘true’ optimal mean returns. This gap can be potentially tightened by HD-BO-RML with a more involved GP design and training (Letham

et al., 2020), or by a multi-output GP which takes into account the correlation between all the objective functions $O(y) := (O_1(y), \dots, O_{n_{RML}}(y)) \sim \text{GP}$. Recently, Dai et al. (2020) derived theoretical guarantees for multi-output GPs in the multi-objective BO setting, as well as practical improvements over the single-output GP approach.

As in Constantine et al. (2015), we can visualize each posterior landscape $p(x|\mathcal{D})$ in the active subspace. Figures 3a, 3d, 3g and 3j show 10000 prior samples $x_i \sim p(x)$ projected into the true two-dimensional (for Figs 3a, 3d, 3g) and one-dimensional (Fig 3j) active subspace coloured by their unnormalized log-posterior density, i.e.,

$$\{A^T x_i, p(x_i|\mathcal{D})\}_{i=1}^{10000}.$$

Indeed, points that have similar posterior densities are close in the active subspace representation.

We expect that the $n_{RML} = 20$ RML samples will be situated in the high posterior density regions. We use our oracle optimizer with access to an unlimited amount of simulator evaluations to obtain ‘true’ RML samples. The resulting samples (projected into the true active subspace) are shown in Figures 3b, 3e, 3h and 3k. We see that samples cover well the high posterior density regions in all the experiments, according to the active subspace representation.

In Figures 3c, 3f, 3i and 3l, we show the analogue samples obtained from using HD-BO-RML instead of the oracle optimizer, averaged over the 5 trials presented in Table 1. While we note a slight difference with the ‘true’ RML samples, as suggested by the mean return gap from Table 1, we see that the HD-BO-RML samples are nonetheless relatively close to the oracle samples in the active subspace representation, and still cover the high posterior density regions well. For the HIV experiment with a one-dimensional active subspace, the HD-BO-RML samples seem to correspond exactly to the ‘true’ RML samples, according to the active subspace representation. Finally, whilst there is some variance between samples from different trials due to the different random embeddings used, the HD-BO-RML samples belong to the high posterior density regions in all the trials. See Appendix C for plots containing the HD-BO-RML samples from every trial.

4. Conclusion

We propose HD-BO-RML, in which we use the HD-BO machinery to tackle the multi-objective RML methodology for posterior sampling. To the best of our knowledge, this is the first GP based approach for high-dimensional posterior sampling in the widespread setting of log-likelihoods with an active subspace, dealing with the challenging case where we do not have access to the active subspace nor have enough computational budget to estimate it. As demonstrated in the

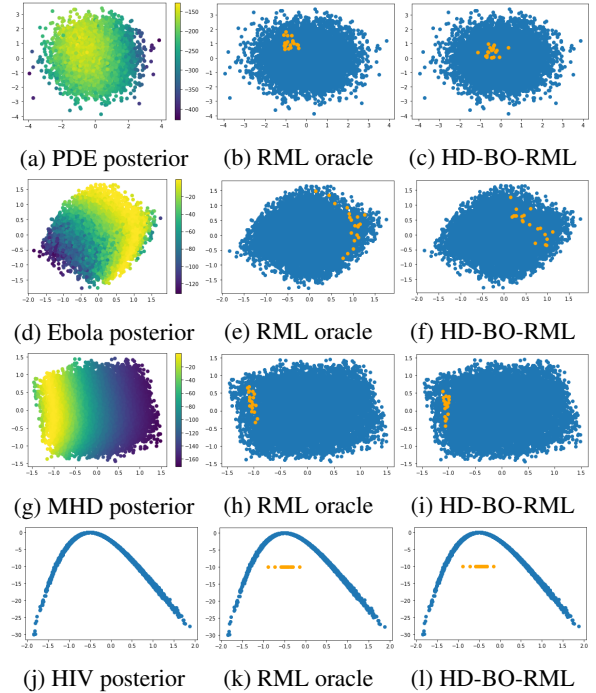


Figure 3. Each row gives results for one simulator. The columns are the approximate posterior landscape in the true active subspace (left); the oracle samples obtained via RML with unlimited computational budget (middle); samples from HD-BO-RML (averaged over the 5 trials from Table 1) (right). The oracle RML and HD-BO-RML samples are shown in orange, with prior samples given in blue. For better visualization in the HIV experiment with a 1D active subspace, the RML samples from the x-axes are shifted towards the middle of figures 3k and 3l.

experiments arising from various domains, the methodology can outperform alternative gradient-free optimization methods and has potential to be used in many real-world applications.

To demonstrate the potential of HD-BO-RML, we presented a vanilla version using default choices of embeddings, GP approximations, and acquisition function etc. By specializing these aspects, further performance gains could be made. In addition to the suggestions in the main text, which mostly refer to developing a more accurate HD-BO procedure, we could also look at removing the active subspace assumption by replacing the random embeddings with an alternative HD-BO methodology that does not require this assumption, such as trust region BO (TurBO) (Eriksson et al., 2019), which uses local GP models in high-dimensions. Moreover, the ad-hoc procedure from Algorithm 3 for combining BO with local optimization could be replaced by the more principled approach from McLeod et al. (2018). Finally, it would be interesting to extend the findings of Dai et al. (2020) regarding multi-objective BO with multi-output GPs to our methodology and to the HD-BO setting in general.

References

- Ardizzone, L., Kruse, J., Wirkert, S., Rahner, D., Pellegrini, E. W., Klessen, R. S., Maier-Hein, L., Rother, C., and Köthe, U. Analyzing Inverse Problems with Invertible Neural Networks. *arXiv e-prints*, art. arXiv:1808.04730, August 2018.
- Ba, Y., de Wiljes, J., Oliver, D. S., and Reich, S. Randomized maximum likelihood based posterior sampling. *arXiv e-prints*, art. arXiv:2101.03612, January 2021.
- Bardsley, J. M., Solonen, A., Haario, H., and Laine, M. Randomize-then-optimize: A method for sampling from posterior distributions in nonlinear inverse problems. *SIAM Journal on Scientific Computing*, 36(4):A1895–A1910, 2014. doi: 10.1137/140964023. URL <https://doi.org/10.1137/140964023>.
- Bilionis, I. and Zabarar, N. Solution of inverse problems with limited forward solver evaluations: A bayesian perspective. *Inverse Problems*, 30, 01 2014. doi: 10.1088/0266-5611/30/1/015004.
- Bilionis, I., Tripathy, R., and Gonzalez, M. Gaussian processes with built-in dimensionality reduction: Applications in high-dimensional uncertainty propagation. *arXiv e-prints*, art. arXiv:1602.04550, February 2016.
- Binois, M. *Uncertainty quantification on pareto fronts and high-dimensional strategies in bayesian optimization, with applications in multi-objective automotive design*. Theses, Ecole Nationale Supérieure des Mines de Saint-Etienne, December 2015. URL <https://tel.archives-ouvertes.fr/tel-01310521>.
- Cartis, C., Fiala, J., Marteau, B., and Roberts, L. Improving the Flexibility and Robustness of Model-Based Derivative-Free Optimization Solvers. *arXiv e-prints*, art. arXiv:1804.00154, March 2018.
- Cleary, E., Garbuno-Inigo, A., Lan, S., Schneider, T., and Stuart, A. M. Calibrate, emulate, sample. *Journal of Computational Physics*, 424:109716, 2021. ISSN 0021-9991. doi: <https://doi.org/10.1016/j.jcp.2020.109716>. URL <https://www.sciencedirect.com/science/article/pii/S0021999120304903>.
- Constantine, P. and Howard, R. Active subspaces data sets. <https://github.com/paulcon/as-data-sets>.
- Constantine, P. G., Dow, E., and Wang, Q. Active subspace methods in theory and practice: applications to kriging surfaces. *arXiv e-prints*, art. arXiv:1304.2070, April 2013.
- Constantine, P. G., Kent, C., and Bui-Thanh, T. Accelerating MCMC with active subspaces. *arXiv e-prints*, art. arXiv:1510.00024, September 2015.
- Dai, S., Song, J., and Yue, Y. Multi-task bayesian optimization via gaussian process upper confidence bound. 2020.
- Diaz, P., Constantine, P., Kalmbach, K., Jones, E., and Pankavich, S. A Modified SEIR Model for the Spread of Ebola in Western Africa and Metrics for Resource Allocation. *arXiv e-prints*, art. arXiv:1603.04955, March 2016.
- Duncan, A. B., Stuart, A. M., and Wolfram, M.-T. Ensemble Inference Methods for Models With Noisy and Expensive Likelihoods. *arXiv e-prints*, art. arXiv:2104.03384, April 2021.
- Dunlop, M. M. and Stuart, A. M. The bayesian formulation of eit: Analysis and algorithms. *arXiv: Probability*, 2015.
- Emerick, A. and Reynolds, A. Investigation of the sampling performance of ensemble-based methods with a simple reservoir model. *Computational Geosciences*, 17, 04 2013. doi: 10.1007/s10596-012-9333-z.
- Eriksson, D., Pearce, M., Gardner, J., Turner, R. D., and Poloczek, M. Scalable global optimization via local bayesian optimization. In Wallach, H., Larochelle, H., Beygelzimer, A., d'Alché-Buc, F., Fox, E., and Garnett, R. (eds.), *Advances in Neural Information Processing Systems*, volume 32. Curran Associates, Inc., 2019. URL <https://proceedings.neurips.cc/paper/2019/file/6c990b7aca7bc7058f5e98ea909e924b-Paper.pdf>.
- Evensen, G. Analysis of iterative ensemble smoothers for solving inverse problems. *Computational Geosciences*, 22, 06 2018. doi: 10.1007/s10596-018-9731-y.
- Forneron, J.-J. and Ng, S. A Likelihood-Free Reverse Sampler of the Posterior Distribution. *arXiv e-prints*, art. arXiv:1506.04017, June 2015.
- Frazier, P. I. A Tutorial on Bayesian Optimization. *arXiv e-prints*, art. arXiv:1807.02811, July 2018.
- Gao, G. and Reynolds, A. Quantifying uncertainty for the punq-s3 problem in a bayesian setting with rml and enkf. *SPE Journal*, 11:506–515, 12 2006. doi: 10.2118/93324-MS.
- Garbuno-Inigo, A., Nüsken, N., and Reich, S. Affine invariant interacting Langevin dynamics for Bayesian inference. *arXiv e-prints*, art. arXiv:1912.02859, December 2019.

- Garbuno-Inigo, A., Hoffmann, F., Li, W., and Stuart, A. M. Interacting langevin diffusions: Gradient structure and ensemble kalman sampler. *SIAM J. Appl. Dyn. Syst.*, 19: 412–441, 2020.
- Glaws, A., Constantine, P. G., Shadid, J., and Wildey, T. M. Dimension reduction in MHD power generation models: dimensional analysis and active subspaces. *arXiv e-prints*, art. arXiv:1609.01255, September 2016.
- Goh, H., Sherifdeen, S., Wittmer, J., and Bui-Thanh, T. Solving Bayesian Inverse Problems via Variational Autoencoders. *arXiv e-prints*, art. arXiv:1912.04212, December 2019.
- Hamdi, H., Couckuyt, I., Costa Sousa, M., and Dhaene, T. Gaussian processes for history-matching: application to an unconventional gas reservoir. *Computational Geosciences*, 21, 04 2017. doi: 10.1007/s10596-016-9611-2.
- Hansen, N., Akimoto, Y., and Baudis, P. CMA-ES/pycma on Github. Zenodo, DOI:10.5281/zenodo.2559634, February 2019. URL <https://doi.org/10.5281/zenodo.2559634>.
- Holden, P. B., Edwards, N. R., Hensman, J. S., and Wilkinson, R. D. Abc for climate: Dealing with expensive simulators. *Handbook of Approximate Bayesian Computation*, 2018.
- Iglesias, M. and Yang, Y. Adaptive regularisation for ensemble kalman inversion. *Inverse Problems*, 37, 12 2020. doi: 10.1088/1361-6420/abd29b.
- Iglesias, M. A., Lu, Y., and Stuart, A. M. A Bayesian Level Set Method for Geometric Inverse Problems. *arXiv e-prints*, art. arXiv:1504.00313, March 2015.
- Iglesias, M. A., Park, M., and Tretyakov, M. V. Bayesian inversion in resin transfer molding. *Inverse Problems*, 2018.
- Ikonomov, B. and Gutmann, M. U. Robust Optimisation Monte Carlo. *arXiv e-prints*, art. arXiv:1904.00670, April 2019.
- Ju, L., Zhang, J., Meng, L., Wu, L., and Zeng, L. An adaptive gaussian process-based iterative ensemble smoother for data assimilation. *Advances in Water Resources*, 115: 125–135, 03 2018. doi: 10.1016/j.advwatres.2018.03.010.
- Kandasamy, K., Schneider, J., and Póczos, B. Query Efficient Posterior Estimation in Scientific Experiments via Bayesian Active Learning. *arXiv e-prints*, art. arXiv:1702.01145, February 2017.
- Letham, B., Calandra, R., Rai, A., and Bakshy, E. Re-Examining Linear Embeddings for High-Dimensional Bayesian Optimization. *arXiv e-prints*, art. arXiv:2001.11659, January 2020.
- Liu, X. and Guillas, S. Dimension reduction for emulation: application to the influence of bathymetry on tsunami heights. *SIAM/ASA Journal on Uncertainty Quantification*, 5, 03 2016. doi: 10.1137/16M1090648.
- Liu, Y., Sun, W., and Durlafsky, L. A deep-learning-based geological parameterization for history matching complex models. *Mathematical Geosciences*, 51, 03 2019. doi: 10.1007/s11004-019-09794-9.
- Loudon, T. and Pankavich, S. Mathematical Analysis and Dynamic Active Subspaces for a Long term model of HIV. *arXiv e-prints*, art. arXiv:1604.04588, April 2016.
- Ma, Y., Dixit, V., Innes, M. J., Guo, X., and Rackauckas, C. A comparison of automatic differentiation and continuous sensitivity analysis for derivatives of differential equation solutions. In *2021 IEEE High Performance Extreme Computing Conference (HPEC)*, pp. 1–9. IEEE, 2021.
- McLeod, M., Osborne, M. A., and Roberts, S. J. Optimization, fast and slow: optimally switching between local and bayesian optimization. *ArXiv*, abs/1805.08610, 2018.
- Meeds, E. and Welling, M. Optimization Monte Carlo: Efficient and Embarrassingly Parallel Likelihood-Free Inference. *arXiv e-prints*, art. arXiv:1506.03693, June 2015.
- Nayebi, A., Munteanu, A., and Poloczek, M. A framework for Bayesian optimization in embedded subspaces. In Chaudhuri, K. and Salakhutdinov, R. (eds.), *Proceedings of the 36th International Conference on Machine Learning*, volume 97 of *Proceedings of Machine Learning Research*, pp. 4752–4761. PMLR, 09–15 Jun 2019. URL <https://proceedings.mlr.press/v97/nayebi19a.html>.
- Oliver, D. S. Metropolized Randomized Maximum Likelihood for sampling from multimodal distributions. *arXiv e-prints*, art. arXiv:1507.08563, July 2015.
- Oliver, D. S., He, N., and Reynolds, A. C. Conditioning permeability fields to pressure data. 1996.
- Powell, M. J. D. A view of algorithms for optimization without derivatives 1. 2007.
- Rasmussen, C. E. and Williams, C. K. I. *Gaussian Processes for Machine Learning (Adaptive Computation and Machine Learning)*. The MIT Press, 2005. ISBN 026218253X.

- Reich, S. and Weissmann, S. Fokker-Planck particle systems for Bayesian inference: Computational approaches. *arXiv e-prints*, art. arXiv:1911.10832, November 2019.
- Seshadri, P., Shahpar, S., Constantine, P., Parks, G., and Adams, M. Turbomachinery Active Subspace Performance Maps. *Journal of Turbomachinery*, 140(4), 01 2018. ISSN 0889-504X. doi: 10.1115/1.4038839. URL <https://doi.org/10.1115/1.4038839>. 041003.
- Siahkoohi, A., Rizzuti, G., Louboutin, M., Witte, P. A., and Herrmann, F. J. Preconditioned training of normalizing flows for variational inference in inverse problems. *arXiv e-prints*, art. arXiv:2101.03709, January 2021.
- Skjervheim, J.-a. and Evensen, G. An ensemble smoother for assisted history matching. *SPE 141929, presented at the SPE Reservoir Simulation Symposium*, 2, 02 2011. doi: 10.2118/141929-MS.
- Srinivas, N., Krause, A., Kakade, S. M., and Seeger, M. Gaussian Process Optimization in the Bandit Setting: No Regret and Experimental Design. *arXiv e-prints*, art. arXiv:0912.3995, December 2009.
- Stuart, A. M. Inverse problems: A bayesian perspective. *Acta Numerica*, 19:451–559, 2010. doi: 10.1017/S0962492910000061.
- Takhtaganov, T. and Müller, J. Adaptive Gaussian process surrogates for Bayesian inference. *arXiv e-prints*, art. arXiv:1809.10784, September 2018.
- Tang, M., Liu, Y., and Durlofsky, L. J. A deep-learning-based surrogate model for data assimilation in dynamic subsurface flow problems. *Journal of Computational Physics*, 413:109456, July 2020. doi: 10.1016/j.jcp.2020.109456.
- Tian, L., Wilkinson, R., Yang, Z., Power, H., Fagerlund, F., and Niemi, A. Gaussian process emulators for quantifying uncertainty in co2 spreading predictions in heterogeneous media. *Computers & Geosciences*, 105:113–119, 2017. ISSN 0098-3004. doi: <https://doi.org/10.1016/j.cageo.2017.04.006>. URL <https://www.sciencedirect.com/science/article/pii/S0098300416304009>.
- Wang, H. and Li, J. Adaptive Gaussian process approximation for Bayesian inference with expensive likelihood functions. *arXiv e-prints*, art. arXiv:1703.09930, March 2017.
- Wang, Z., Hutter, F., Zoghi, M., Matheson, D., and de Freitas, N. Bayesian Optimization in a Billion Dimensions via Random Embeddings. *arXiv e-prints*, art. arXiv:1301.1942, January 2013.
- Wycoff, N., Binois, M., and Wild, S. M. Sequential Learning of Active Subspaces. *arXiv e-prints*, art. arXiv:1907.11572, July 2019.
- Yashchuk, I. Bringing {pde}s to {jax} with forward and reverse modes automatic differentiation. In *ICLR 2020 Workshop on Integration of Deep Neural Models and Differential Equations*, 2020. URL <https://openreview.net/forum?id=nEPNoiGsU3>.

A. Proof for the linear simulator case

In case of a linear simulator $f(x) := Hx$, Gaussian prior distribution $x \sim \mathcal{N}(\mu, \Sigma)$, and Gaussian likelihood $\mathcal{D}|x \sim \mathcal{N}(Hx, \Sigma_{\text{obs}})$, the posterior distribution $p(x|\mathcal{D})$ is also Gaussian:

$$x|\mathcal{D} \sim \mathcal{N}(m, V),$$

where

$$V = (\Sigma^{-1} + H^\top \Sigma_{\text{obs}}^{-1} H)^{-1}$$

and $m = V(\Sigma^{-1} \mu + H^\top \Sigma_{\text{obs}}^{-1} \mathcal{D})$.

To see why randomized maximum likelihood (RML) from Algorithm 1 produces exact samples from the posterior distribution in this case, we first recall the RML objective functions from (1):

$$O_n(x) := \log \mathcal{N}_m(Hx|\mathcal{D}_n, \Sigma_{\text{obs}}) + \log \mathcal{N}_D(x|\mu_n, \Sigma),$$

where $\mu_n := \mu + \epsilon_n$ and $\mathcal{D}_n := \mathcal{D} + \eta_n$, with $\epsilon_n \sim \mathcal{N}(0, \Sigma)$ and $\eta_n \sim \mathcal{N}(0, \Sigma_{\text{obs}})$.

Differentiating with respect to x gives

$$\nabla O_n(x) = 2\Sigma^{-1}x - 2\Sigma^{-1}\mu_n + 2H^\top \Sigma_{\text{obs}}^{-1}Hx - 2H^\top \Sigma_{\text{obs}}^{-1}\mathcal{D}_n$$

and setting this equal to zero and rearranging gives

$$\begin{aligned} x &= (\Sigma^{-1} + H^\top \Sigma_{\text{obs}}^{-1} H)^{-1} (\Sigma^{-1} \mu_n + H^\top \Sigma_{\text{obs}}^{-1} \mathcal{D}_n) \\ &= m + V(\Sigma^{-1} \epsilon_n + H^\top \Sigma_{\text{obs}}^{-1} \eta_n). \end{aligned}$$

The distribution of x can then easily be seen to be

$$\begin{aligned} x &\sim \mathcal{N}(m, V(\Sigma^{-1} \Sigma \Sigma^{-1} + H^\top \Sigma_{\text{obs}}^{-1} \Sigma_{\text{obs}} \Sigma_{\text{obs}}^{-1} H) V^\top) \\ &= \mathcal{N}(m, V), \end{aligned}$$

i.e., x is a sample from the true posterior distribution.

B. Additional implementation details

B.1. Local prior optimization in Algorithm 4

For each local optimization step of the Gaussian prior distribution in Algorithm 4, we have used the CMA-ES algorithm starting at the point selected by maximizing the HD-BO acquisition function $x_0 = R_k y_n^k$, together with a standard deviation of 0.1. Note that in our experiments $x \sim \mathcal{N}(0, I_D)$, so the CMA-ES standard deviation for optimization is 10 times smaller than the prior standard deviation. We have also restricted the number of (prior) function evaluations performed by CMA-ES to a maximum of 500, in order to prevent the points being too far away from x_0 , which would lead to a severe decrease in the log-likelihood.

B.2. Competing optimization methods

For the uniform prior experiments, we use the prior box constraints $[a_i, b_i]_{i=1}^D \rightarrow [-1, 1]^D$ for CMA-ES and BOBYQA optimization. We use the center 0_D of the (transformed) box $[-1, 1]^D$ as the starting point for CMA-ES, together with a standard deviation of $1/3$ such that 3 standard deviations cover the entire box. For BOBYQA, we use a starting point sampled at random from $[-1, 1]^D$.

For the Gaussian prior experiment with $x \sim \mathcal{N}(0, I_D)$, we use the mean 0_D as the starting point for CMA-ES, together with a standard deviation of 1. For BOBYQA, we use a starting point sampled at random from a $\mathcal{N}(0, I_D)$ distribution.

B.3. HD-BO-RML implementation

For HD-BO-RML (Algorithm 3 and 4) we use $K = 10$ random embeddings, sampled as described in the Subsection 3.1. We decided to choose a relatively large number of embeddings in order to encourage a good coverage of the high posterior density regions, as some random embeddings might get stuck in the exploitation phase and select samples from the same region for all the RML objectives.

We choose $d_e = d = 2$ for the Gaussian prior (Elliptic-PDE) experiment, i.e., the dimension of the random embedding is the same as for the true active subspace, and $d_e = d + 1$ for all the other experiments, i.e., the dimension of the random embedding is slightly larger than the true active subspace. These choices are common in the HD-BO literature.

In the uniform prior experiments, we select $n_0 = 5$ initial points $y \in \mathbb{R}^{d_e}$ from $[-1, 1]^{d_e}$, using rejection sampling to ensure that they project back to the (transformed) prior box $[a_i, b_i]_{i=1}^D \rightarrow [-1, 1]^D$ (i.e. $-1 \leq (R_k y)_d \leq 1$ for all $d \in [D]$), as suggested in Letham et al. (2020). For the Gaussian prior experiment with $x \sim \mathcal{N}(0, I_D)$, we select $n_0 = 5$ initial points $y \in \mathbb{R}^{d_e}$, sampled at random from a $\mathcal{N}(0, I_{d_e})$ distribution. As discussed in Subsection 3.1, using rejection sampling from $[-\sqrt{d_e}, \sqrt{d_e}]^{d_e}$ (uniform prior) or sampling from $\mathcal{N}(0, (\sqrt{d_e})^2 I_{d_e})$ (Gaussian prior) is generally more appropriate, as $y \in [-\sqrt{d_e}, \sqrt{d_e}]^{d_e}$ is likely to project back to $R_k y \in [-1, 1]^D$. Nonetheless, in the experiments considered here $d_e \in \{2, 3\}$ (thus $\sqrt{d_e}$ is close to 1), and so the difference should not be too significant (in the worst case scenario, our initial points cover less of the prior space than the generally more appropriate design).

C. HD-BO-RML samples for all the trials

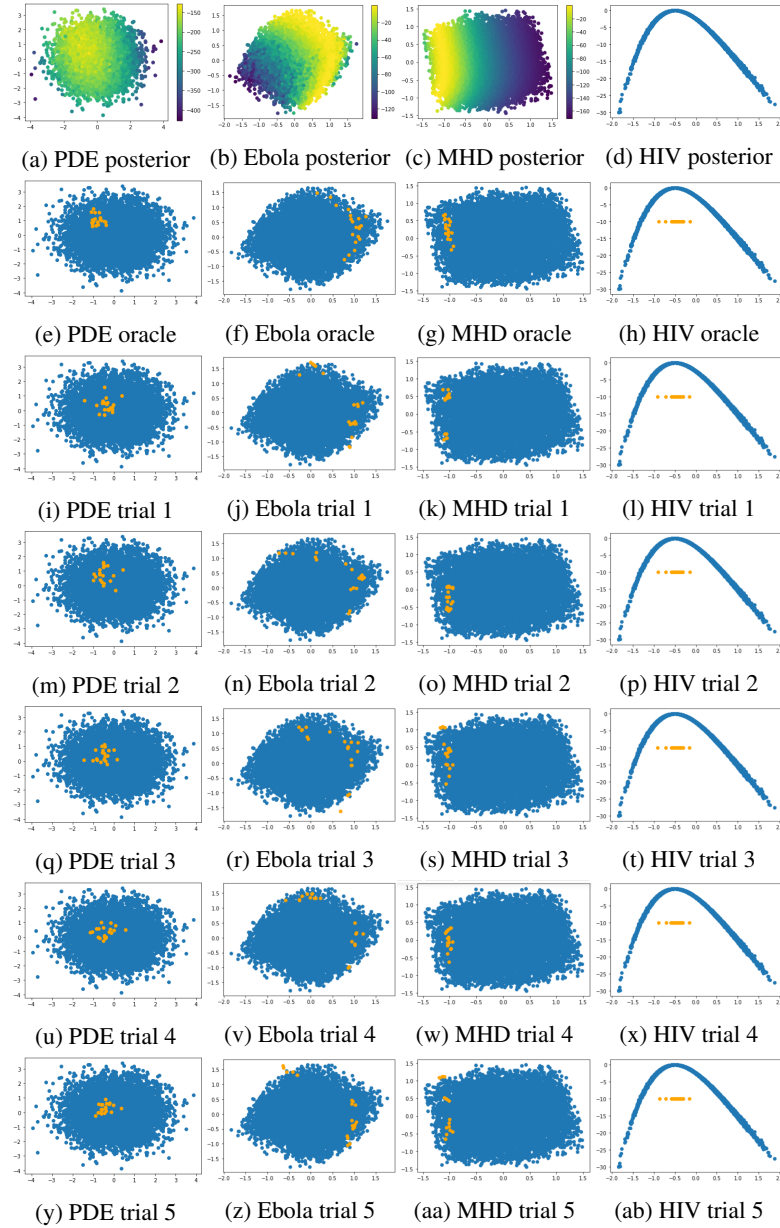


Figure 4. Each column gives results for one simulator. The rows are the approximate posterior landscape in the true active subspace (first row); the oracle samples obtained via RML with unlimited computational budget (second row); samples from HD-BO-RML for the 5 trials presented in Table 1 (third to seventh row). The oracle RML and HD-BO-RML samples are shown in orange, with prior samples given in blue. For better visualization in the HIV experiment with a 1D active subspace, the RML samples from the x-axis are shifted towards the middle of the HIV plots.